

# Optimizing quantum violation for multipartite facet Bell inequalities

Jin-Fu Chen (陈劲夫) <sup>1, 2, \*</sup> Mengyao Hu (胡梦瑶) <sup>1, 2, †</sup> and Jordi Tura <sup>1, 2, ‡</sup>

<sup>1</sup>*Instituut-Lorentz, Universiteit Leiden, P.O. Box 9506, 2300 RA Leiden, The Netherlands*

<sup>2</sup> *$\langle aQa^L \rangle$  Applied Quantum Algorithms, Universiteit Leiden, The Netherlands*

(Dated: November 12, 2025)

Nonlocality shapes quantum correlations, revealed through the violation of Bell inequalities. The intersection of all valid Bell inequalities is the so-called local polytope. In multipartite systems, characterizing the local polytope quickly becomes an intractable task as the system size increases. Optimizing Bell inequalities to maximize the ratio between their quantum value and classical bound is key to understanding multipartite nonlocality. We propose a gradient-based method for this optimization. Numerical results indicate that local maxima of this ratio typically correspond to facet Bell inequalities of the local polytope. This enables an iterative search for tight and robust Bell inequalities. Applied to permutation-invariant scenarios, the method provides tight Bell inequalities with large quantum violations and facilitates experimental certification of Bell correlations without full knowledge of the local polytope.

*Introduction.*—Bell inequalities serve as fundamental tools for detecting quantum nonlocality, the inability of local hidden variable theories to reproduce all quantum predictions [1, 2]. Among them, the Clauser-Horne-Shimony-Holt (CHSH) inequality is the most studied and experimentally tested Bell inequality [3]. It provides a clear signature of nonlocal correlations in bipartite systems [4, 5], where recent breakthroughs have enabled loophole-free tests [6–10]. Beyond its foundational significance, nonlocality has emerged as a critical resource for device-independent quantum information protocols, including quantum key distribution [11–14], certified randomness generation [15–17], and quantum system verification through self-testing [18–20].

Generalizing Bell nonlocality to the multipartite regime poses significant conceptual and practical challenges. As the number of parties increases, while the settings per party remain fixed, the number of correlation terms grows exponentially, and the complexity of characterizing the local polytope grows as  $O((\exp N)^{(\exp N)})$  [21], rendering a complete characterization of multipartite nonlocality intractable [22–24]. The local polytope, defined as the intersection of all valid Bell inequalities [25], can be characterized either by its vertices or its facets. Although generating the vertices is straightforward, the number grows exponentially with the number of parties. Deriving the corresponding facets quickly becomes computationally intractable [21, 26]. A practical approach is to restrict to few-body correlators and exploit symmetries, thereby greatly reducing the number of free coefficients in Bell inequalities and constraining the structure of correlations [27–29]. For instance, permutation symmetry among parties allows the construction of symmetric Bell inequalities that detect nonlocality in physically relevant many-body systems [30, 31], while remaining analytically and numerically tractable [27, 32]. Symmetry thus provides a promising route to construct scalable and experimentally relevant Bell inequalities for many-body systems [33, 34].

To characterize multipartite Bell nonlocality, it is essential to optimize Bell inequalities to enhance the gap between the classical bound and the quantum value. Such optimized inequalities are particularly useful in experiments, as larger separation generally implies greater robustness to noise and improved feasibility in experimental implementations [34–36]. In addition to enhancing the quantum–classical gap, identifying tight Bell inequalities that define facets of the local polytope is also important, as they set the fundamental limits of classical correlations, and all facets together form the minimal description of correlations consistent with a local hidden-variable model. However, current methods for identifying these robust and tight Bell inequalities face significant limitations. Recent approaches leveraging machine learning techniques [37] and iterative optimization methods [36] have shown potential, but these methods exhibit limited scalability and fail to characterize complex polytopes.

In this Letter, we propose a gradient-based method to optimize Bell inequalities by enhancing the ratio between the quantum value for a fixed Hilbert space dimension, and the classical bound. We observe that the method converges to a local maximum of this ratio that corresponds to a tight Bell inequality. It simultaneously determines the classical bound, the measurement settings, and the quantum state achieving the quantum violation corresponding to such local maximum. We focus on the  $(N, m, 2)$  scenario, where each of the  $N$  parties performs one of  $m$  possible measurements with binary outcomes  $\pm 1$ . As a first benchmark, our optimization reproduces the CHSH inequality in the symmetrized  $(2, 2, 2)$  scenario. We then apply it to the permutation-invariant (PI) Bell inequalities consisting of up to two-body correlators for general  $(N, m, 2)$  scenarios with  $m = 2$  and 3. Our approach avoids enumerating all facets of the corresponding local polytope at once, a task that becomes intractable due to the exponential complexity with  $N$ . We identify families of tight Bell inequalities for  $m = 2$

and 3, and obtain previously unknown tight Bell inequalities for  $m = 3$ . Finally, we verify the maximum ratio on the affine projections and cross sections of both the primal and dual spaces, which reveals geometric insight into multipartite nonlocality.

*Setup.*—A Bell inequality is given by a linear functional of the probability distribution  $I = \sum_{\mathbf{a}, \mathbf{x}} T_{\mathbf{a}, \mathbf{x}} P(\mathbf{a}|\mathbf{x}) \geq \beta_C$ , where the coefficients  $T_{\mathbf{a}, \mathbf{x}} \in \mathbb{R}$  specify the inequality,  $P(\mathbf{a}|\mathbf{x})$  denotes the conditional probability of obtaining outcomes  $\mathbf{a} = (a_1, \dots, a_N)$  with  $a_i = 0$  or 1 given measurement settings  $\mathbf{x} = (x_1, \dots, x_N)$  with  $x_i \in [m] = \{0, \dots, m-1\}$ . The classical bound  $\beta_C$  is defined as the minimum of  $I$  over all local behaviors,  $\beta_C = \min_{\vec{P} \in \mathcal{L}} I$ , and  $\vec{P} = \{P(\mathbf{a}|\mathbf{x})\}_{\mathbf{a}, \mathbf{x}}$  [38], where  $\mathcal{L}$  is the local polytope. The inequality is tight when the saturating local behaviors define a facet of the polytope  $\mathcal{L}$ , i.e., a supporting hyperplane of maximal dimension. We reformulate the linear functional in the correlator space as

$$I = \sum_{\boldsymbol{\mu}} \alpha_{\boldsymbol{\mu}} \langle A_{\boldsymbol{\mu}} \rangle, \quad (1)$$

where the composite index  $\boldsymbol{\mu}$  labels the  $\ell$ -body correlator  $A_{\boldsymbol{\mu}} = A_{x_{i_1}}^{(i_1)} \cdots A_{x_{i_\ell}}^{(i_\ell)}$  acting on the sites  $i_1, i_2, \dots, i_\ell$ . The inputs on these sets are given by  $\mathbf{x}_\ell = (x_{i_1}, \dots, x_{i_\ell}) \in [m]^\ell$ . For binary outcomes, the correlator is defined by  $\langle A_{\boldsymbol{\mu}} \rangle = \sum_{\mathbf{a}_\ell} (-1)^{\sum_{j=1}^\ell a_{i_j}} P(\mathbf{a}_\ell|\mathbf{x}_\ell)$  with  $\mathbf{a}_\ell = (a_{i_1}, \dots, a_{i_\ell})$ . The coefficient of each correlator is given by  $\alpha_{\boldsymbol{\mu}} \in \mathbb{R}$  [28, 39, 40]. The classical bound of the Bell inequality can be rewritten in correlator form as  $\beta_C = \min_{\langle A_{\boldsymbol{\mu}} \rangle \in \mathcal{L}} I$ , where  $\mathcal{L}$  now denotes the local polytope in the correlator space.

In the quantum case, the linear functional (1) corresponds to the expectation value of Bell operators on a quantum state, and such operators can be interpreted as a Hamiltonian in quantum many-body systems. The spectral properties of these Hamiltonians, in particular their ground state energies, quantify multipartite nonlocality with a fixed Hilbert space dimension [39, 41–43]. For an  $N$ -partite pure  $|\psi\rangle$ , the expectation of the correlator is given by  $\langle \hat{A}_{\boldsymbol{\mu}} \rangle = \langle \psi | \hat{A}_{\boldsymbol{\mu}} | \psi \rangle$ . Note that observables  $\hat{A}_{\boldsymbol{\mu}}$  are parameterized by the measurement setting  $\boldsymbol{\theta} = \{\theta_x^{(i)}\}_{i, x}$  and acts as a Hermitian operator on the Hilbert space with a fixed dimension. By specifying all measurement settings, one defines the Bell operator  $\hat{I}(\boldsymbol{\theta})$ . The minimum quantum value is obtained by optimizing over all measurement settings and states  $\beta_Q = \min_{\boldsymbol{\theta}, |\psi\rangle} \langle \psi | \hat{I}(\boldsymbol{\theta}) | \psi \rangle := \langle \psi^* | \hat{I}(\boldsymbol{\theta}^*) | \psi^* \rangle$ , where  $|\psi^*\rangle$  is the ground state and  $\boldsymbol{\theta}^* = \{\theta_x^{(i)*}\}_{i, x}$  is the optimal measurement setting that minimize the ground-state energy. To minimize the quantum value  $\beta_Q$ , we compute its gradient with respect to the measurement parameters

$\boldsymbol{\theta}$ . The derivatives are given by [44]

$$\frac{\partial}{\partial \theta_x^{(i)}} \langle \psi^* | \hat{I}(\boldsymbol{\theta}) | \psi^* \rangle = \langle \psi^* | \frac{\partial \hat{I}(\boldsymbol{\theta})}{\partial \theta_x^{(i)}} | \psi^* \rangle. \quad (2)$$

A Bell inequality is nontrivial if  $\beta_Q/\beta_C > 1$ , meaning that some quantum states and measurements lead to violations of the classical bound  $\beta_C$ .

*Ratio optimization.*—We define the ratio  $\Delta := \beta_Q/\beta_C$  that characterizes the potential of a Bell inequality to certify nonlocal correlations, with larger values indicating greater robustness to noise. By optimizing the coefficients  $\alpha_{\boldsymbol{\mu}}$ , we maximize the ratio  $\Delta$ , and our numerical results indicate that the local maxima typically correspond to facet Bell inequalities.

Note that  $\beta_Q$  is a piecewise-smooth function with respect to the coefficients  $\alpha_{\boldsymbol{\mu}}$ , and its derivatives are given by [44]

$$\frac{\partial \beta_Q}{\partial \alpha_{\boldsymbol{\mu}}} = \langle \psi^* | \frac{\partial \hat{I}(\boldsymbol{\theta})}{\partial \alpha_{\boldsymbol{\mu}}} \Big|_{\boldsymbol{\theta}=\boldsymbol{\theta}^*} | \psi^* \rangle. \quad (3)$$

For the classical bound  $\beta_C$ , kinks occur when the set of saturating vertices changes on the local polytope. From the definition of  $\beta_C$ , at least one vertex saturates the Bell inequality. We fix the classical bound  $\beta_C$  and iteratively add new saturating vertices determined by the gradient direction of  $\beta_Q$ . The coefficients  $\alpha_{\boldsymbol{\mu}}$  are updated along this direction to increase the ratio

$$\frac{\partial \Delta}{\partial \alpha_{\boldsymbol{\mu}}} = \frac{1}{\beta_C} \frac{\partial \beta_Q}{\partial \alpha_{\boldsymbol{\mu}}}, \quad (4)$$

subject to the constraints  $\sum_{\boldsymbol{\mu}} \alpha_{\boldsymbol{\mu}} v_{\boldsymbol{\mu}, j} = \beta_C$ , where  $v_{\boldsymbol{\mu}, j}$  are the vertices saturating the classical bound. Other vertices yield larger classical values than the classical bound  $\sum_{\boldsymbol{\mu}} \alpha_{\boldsymbol{\mu}} \langle A_{\boldsymbol{\mu}} \rangle \geq \beta_C$ . By varying  $\alpha_{\boldsymbol{\mu}}$ , new vertices become active and are added to the constraints, progressively tightening the Bell inequality. A Bell inequality becomes tight when its hyperplane forms a facet of the local polytope, i.e., when it is saturated by a sufficient number of affinely independent vertices. We give the update rule of  $\alpha_{\boldsymbol{\mu}}$  in [44].

The linear functional in Eq. (1) is defined with respect to the origin of correlator space, yet it can also be referenced to other points, e.g.,  $I = \sum_{\boldsymbol{\mu}} \alpha_{\boldsymbol{\mu}} (\langle A_{\boldsymbol{\mu}} \rangle - O_{\boldsymbol{\mu}})$  with some nonzero  $O_{\boldsymbol{\mu}}$ . Our method remains applicable as long as  $O_{\boldsymbol{\mu}}$  lies within the local polytope, in which case the optimization identifies a nearby facet.

*Benchmarking CHSH inequality.*—We start with a bipartite scenario in which each party performs two measurements with two possible outcomes. The linear functional is expressed by the correlators as  $I = \sum_{k, l=0}^1 \alpha_{kl} \langle A_k B_l \rangle$ , where the outcomes of  $A_k$  and  $B_l$  are  $\pm 1$ . For simplicity, we consider the symmetric inequality with  $\alpha_{10} = \alpha_{01}$ . To evaluate the quantum value, we assign the symmetric measurement setting  $\hat{A}_0 = \hat{\sigma}_z^A$ ,

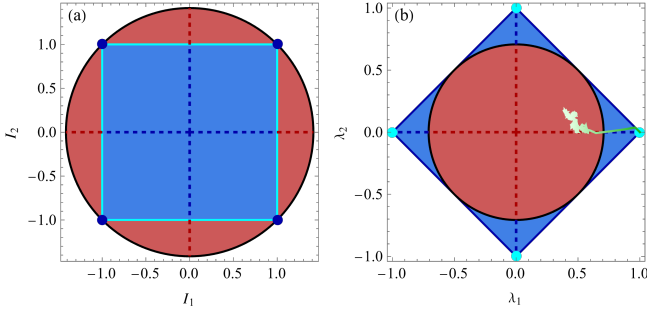


FIG. 1. Illustration of the ratio-optimization procedure for a two-body Bell inequality. The maximal ratio identifies a tight Bell inequality. (a) Local (blue) polytope and quantum (red) convex set in the primal space, projected onto a two-dimensional plane spanned by the linear functionals  $I_1$  and  $I_2$ . Blue dots represent the vertices of the local polytope after projection. (b) Corresponding objects in the dual-space cross-section, where cyan dots represent tight Bell inequalities. In both panels, the dashed curve indicates the tight inequality achieving the largest ratio. The light-green curve shows the projected trajectory of the coefficients  $\alpha_{kl}$  during the optimization, plotted in the  $(\lambda_1, \lambda_2)$  cross-section, demonstrating convergence to a CHSH inequality.

$\hat{B}_0 = \hat{\sigma}_z^B$ ,  $\hat{A}_1 = \cos \theta \hat{\sigma}_z^A + \sin \theta \hat{\sigma}_x^A$ ,  $\hat{B}_1 = \cos \theta \hat{\sigma}_z^B + \sin \theta \hat{\sigma}_x^B$  and obtain the Bell operator  $\hat{I}(\theta)$ .

Figure 1(a) shows a two-dimensional affine projection of the local polytope and the quantum convex set in the primal space of correlators, using the two linear functionals  $I_1 = (\langle A_0 B_0 \rangle + \langle A_0 B_1 \rangle + \langle A_1 B_0 \rangle - \langle A_1 B_1 \rangle)/2$  and  $I_2 = (-\langle A_0 B_0 \rangle + \langle A_0 B_1 \rangle + \langle A_1 B_0 \rangle + \langle A_1 B_1 \rangle)/2$ . Figure 1(b) shows the corresponding dual-space cross-section (the space of Bell functionals up to scale). In general, dual extreme points are represented by coefficients  $\lambda_{\mu} = \alpha_{\mu}/\beta$ , so that the inequality reads  $\sum_{\mu} \lambda_{\mu} \langle A_{\mu} \rangle \geq -1$ . Facet Bell inequalities correspond to vertices of the dual polytope at  $\beta = \beta_C$ ; the dual quantum boundary is obtained at  $\beta = \beta_Q$ . We evaluate  $\beta_C$  and  $\beta_Q$  for the family  $I = \lambda_1 I_1 + \lambda_2 I_2$  spanned by  $I_1$  and  $I_2$ . In the dual space, the admissible region is the set of  $(\lambda_1, \lambda_2)$  such that every point in the primal space satisfies  $\lambda_1 I_1 + \lambda_2 I_2 \geq -1$ .

We then apply our gradient-based optimization to the coefficients  $\alpha_{kl}$ . The light-green curve shows the optimization trajectory (projected onto the dual cross-section), which converges to the CHSH facet, attaining the maximal quantum-to-classical ratio  $\Delta^{\max} = \sqrt{2}$  ( $\beta_Q = -2\sqrt{2}$  vs.  $\beta_C = -2$ ). The initial linear functional is  $I = 0.3\langle A_0 B_1 \rangle + 0.3\langle A_1 B_0 \rangle - 0.5\langle A_1 B_1 \rangle$ , where the gradient vanishes; to escape this flat region we add small random perturbations to the coefficients  $\alpha_{\mu}$  [44].

*Permutation-invariant Bell inequalities.*—Now we focus on PI Bell inequalities involving up to two-body correlators. For the  $(N, m, 2)$  scenario, the linear functional takes the form  $I = \sum_{k=0}^{m-1} \alpha_k \langle \mathcal{S}_k \rangle + \sum_{k,l=0}^{m-1} \alpha_{kl} \langle \mathcal{S}_{kl} \rangle / 2$ , with one- and two-body observables  $\mathcal{S}_k := \sum_{i=1}^N A_k^{(i)}$  and

$\mathcal{S}_{kl} := \sum_{i \neq j} A_k^{(i)} A_l^{(j)}$ , where  $(i), (j)$  label the sites and  $k, l$  denote the measurement. Using  $\mathcal{S}_{kl} = \{\mathcal{S}_k, \mathcal{S}_l\}/2 - \mathcal{Z}_{kl}$ , with  $\mathcal{Z}_{kl} := \sum_{i=1}^N (A_k^{(i)} A_l^{(i)} + A_l^{(i)} A_k^{(i)})/2$  [27, 44], we formally rewrite the linear functional  $I$  as

$$I = \sum_{k=0}^{m-1} \alpha_k \langle \mathcal{S}_k \rangle + \frac{1}{2} \sum_{k,l=0}^{m-1} \alpha_{kl} (\langle \mathcal{S}_k \mathcal{S}_l \rangle - \langle \mathcal{Z}_{kl} \rangle), \quad (5)$$

under the constraint  $-N + |\langle \mathcal{S}_k \rangle + \langle \mathcal{S}_l \rangle| \leq \langle \mathcal{Z}_{kl} \rangle \leq N - |\langle \mathcal{S}_k \rangle - \langle \mathcal{S}_l \rangle|$ . To evaluate the classical bound  $\beta_C$ , we consider the local deterministic strategies for  $\mathcal{S}_k$  and  $\mathcal{Z}_{kl}$ . It is known that vertices of the local polytope are characterized by  $\mathcal{S}_k \in \{-N, -N+2, \dots, N-2, N\}$  and  $\mathcal{Z}_{kl} = -N + |\mathcal{S}_k + \mathcal{S}_l|$  or  $N - |\mathcal{S}_k - \mathcal{S}_l|$  according to the sign of  $\alpha_{kl}$  [27, 44]. For the quantum value, we adopt the symmetric measurement setting with the observables  $\hat{\mathcal{S}}_k = 2 \cos \theta_k \hat{S}_z + 2 \sin \theta_k \hat{S}_x$  and  $\hat{\mathcal{Z}}_{kl} = N \cos(\theta_k - \theta_l)$ , where  $\hat{S}_x$  and  $\hat{S}_z$  are the collective spin operators [27]. Restricting the measurements on qubits and onto the real circle of the Bloch sphere is sufficient to attain the maximum quantum violation for  $m = 2$  by virtue of Jordan's lemma [45]. The quantum value is obtained as the variational minimum of the ground-state energy of the Hamiltonian  $\hat{I}(\theta)$  over different measurement settings  $\theta = \{\theta_k\}_k$ .

We apply our gradient-based optimization to the  $(N, 2, 2)$  scenario [27]. For finite  $N$ , we seek the coefficients  $\alpha_{\mu} = (\alpha_0, \alpha_1, \alpha_{00}, \alpha_{01}, \alpha_{11})$  that maximize the ratio  $\Delta_{N,2}$  and we denote the global maximum ratio for given  $N$  as  $\Delta_{N,2}^{\max}$ . The vertices of the local polytope are the extreme points of the five-dimensional space spanned by  $\langle \mathcal{S}_{\mu} \rangle = (\langle \mathcal{S}_0 \rangle, \langle \mathcal{S}_1 \rangle, \langle \mathcal{S}_{00} \rangle, \langle \mathcal{S}_{01} \rangle, \langle \mathcal{S}_{11} \rangle)$ . In this scenario, the numerical results show that the Bell inequalities become tight when the ratio attains a local maximum. Therefore, optimization of the coefficients can be used to find tight Bell inequalities. For example, for  $N = 3$ , we obtain the tight Bell inequality with coefficients  $\alpha_{\mu} = (6, 2, 6, 3, -2)$ , which reaches the maximum ratio  $\Delta_{3,2}^{\max} = 1.11303$ . For other values of  $N$ , the maximum ratios are summarized in Table I.

We find a family of tight Bell inequalities related to the coefficients

$$\alpha_{\mu} = \alpha_{1,\mu} + n \alpha_{2,\mu}, \quad (6)$$

with  $\alpha_{1,\mu} = (1, -1, 1, 1, 1)$  and  $\alpha_{2,\mu} = (1, 1, 0, 0, 0)$  and  $n \in \{-2N + 7, -2N + 9, \dots, 2N - 9, 2N - 7\}$ . The maximum ratio is reached by  $n = \pm 1$ . Figure 2(a) and (b) show the affine projection and the cross section for this family of tight Bell inequalities for the  $(12, 2, 2)$  scenario, respectively. The cyan dots represent the vertices of the local polytope. The blue and red dashed lines show the classical bound and the quantum value, respectively. This family includes the Bell inequality with coefficients  $(2, 0, 1, 1, 1)$  which achieves the largest ratio as  $N$  increases.

TABLE I: Maximum ratio  $\Delta_{N,2}^{\max}$ , classical bound  $\beta_C$ , and corresponding coefficients for the  $(N, 2, 2)$  scenario.

| $N$ | $\Delta_{N,2}^{\max}$ | $\beta_C$ | $\alpha_{\mu}$     |
|-----|-----------------------|-----------|--------------------|
| 2   | $\sqrt{2}$            | -2        | (0, 0, 1, 1, -1)   |
| 3   | 1.11303               | -18       | (6, 2, 6, 3, -2)   |
| 4   | 1.11302               | -18       | (0, 0, 6, 2, -1)   |
| 5   | 1.05904               | -80       | (20, 4, 20, 5, -2) |
| 6   | 1.05884               | -60       | (0, 0, 15, 3, -1)  |
| 7   | 1.03384               | -14       | (2, 0, 1, 1, 1)    |
| 8   | 1.04058               | -16       | (2, 0, 1, 1, 1)    |
| 9   | 1.04931               | -18       | (2, 0, 1, 1, 1)    |
| 10  | 1.05528               | -20       | (2, 0, 1, 1, 1)    |
| 20  | 1.09814               | -40       | (2, 0, 1, 1, 1)    |
| 30  | 1.12043               | -60       | (2, 0, 1, 1, 1)    |
| 40  | 1.13479               | -80       | (2, 0, 1, 1, 1)    |

We now apply our method to the  $(N, 3, 2)$  scenario. Introducing an additional measurement enables the construction of Bell inequalities with larger ratios, i.e.,  $\Delta_{N,3}^{\max} \geq \Delta_{N,2}^{\max}$ . Thus, these inequalities are more robust and may be easier to certify experimentally. For  $m = 3$ , all tight Bell inequalities can be enumerated only when  $N < 5$  [46], and we list these inequalities in [44]. For larger  $N$ , a complete enumeration is infeasible, but our gradient-based method remains applicable for searching facet Bell inequalities. For small  $N$  we find that  $\Delta_{N,3}^{\max} = \Delta_{N,2}^{\max}$ , while for  $N \geq 4$  the scenario with three measurements indeed leads to a larger ratio  $\Delta_{N,3}^{\max} \geq \Delta_{N,2}^{\max}$ .

We find a family of tight Bell inequalities whose coefficients are given by Eq. (6) with  $\alpha_{1,\mu} = (2, 0, -2, 1, 1, 1, 1, 1, 1)$  and  $\alpha_{2,\mu} = (1, 1, 1, 0, 0, 0, 0, 0, 0)$ , and  $n \in \{-2N+1, -2N+3, \dots, 2N-3, 2N-1\}$  for even  $N$  and  $n \in \{-2N, -2N+2, \dots, 2N-2, 2N\}$  for odd  $N$ , where  $\alpha_{1,\mu}$  corresponds to the Bell inequality considered in Ref. [47]. Figure 2(c) and (d) show the affine projection and the cross section of this family for  $N = 11$ , respectively. Interestingly, we find that for sufficiently large  $N$  the optimal Bell inequality with largest ratio does not belong to this family. For example, for  $N = 141$ , we find  $\alpha_{\mu} = (694, 0, -694, 385, 309, 385, 248, 309, 385)$  with a ratio  $\Delta = 1.21485$ , which exceeds the ratio  $\Delta = 1.21482$  of  $\alpha_{1,\mu}$ . This implies that with more measurements, finding the Bell inequality with the largest ratio is no longer as straightforward as for  $m = 2$ . Nevertheless, our gradient-based method remains effective in identifying inequalities with larger ratios. In Table II, we show some other non-trivial tight Bell inequalities not given by Eq. (6).

TABLE II: Selected tight Bell inequalities for  $m = 3$  with their ratios and classical bounds. These inequalities are distinct from those in the  $m = 2$  scenario.

| $N$ | $\Delta_{N,3}$ | $\beta_C$ | $\alpha_{\mu}$                |
|-----|----------------|-----------|-------------------------------|
| 2   | $5/4$          | -8        | (2, 1, 1, 2, 2, 2, -2, 1, -2) |

(continued on next page)

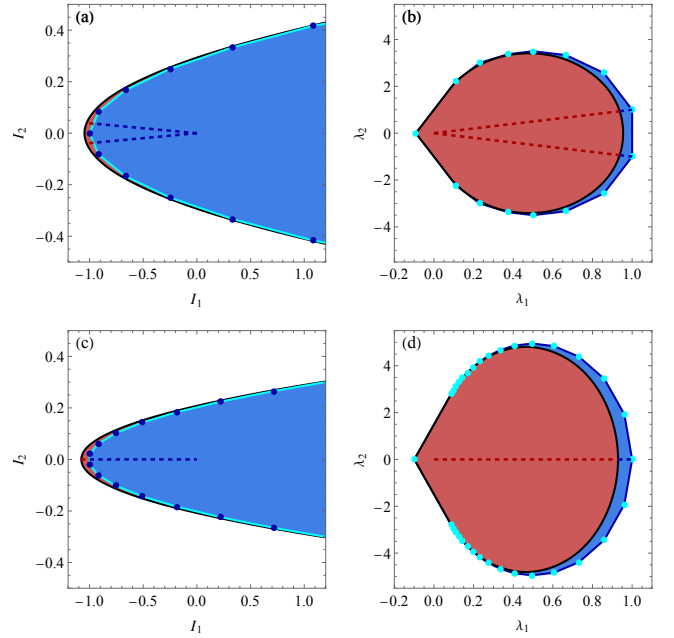


FIG. 2. Two-dimensional affine projections (left) and corresponding cross-sections (right) for the  $(N, m, 2)$  scenarios. (a) and (b)  $N = 12$ ,  $m = 2$ . The projection plane is spanned by the two functionals with coefficients  $\alpha_{1,\mu} = (1, -1, 1, 1, 1)/24$  and  $\alpha_{2,\mu} = (1, 1, 0, 0, 0)/24$ . (c) and (d)  $N = 11$ ,  $m = 3$ . The affine projection is spanned by  $\alpha_{1,\mu} = (2, 0, -2, 1, 1, 1, 1, 1)/49$  and  $\alpha_{2,\mu} = (1, 1, 1, 0, 0, 0, 0, 0)/49$ . Dashed lines indicate the maximum ratio in the affine projections and cross sections. Blue dots (left panels) show the vertices in the primal affine projections and correspond to blue lines (right panels) in the dual cross-sections. Cyan lines (left panels) denote tight Bell facets, which map to cyan vertices (right panels).

(continued from previous page)

| $N$ | $\Delta_{N,3}$ | $\beta_C$ | $\alpha_{\mu}$                         |
|-----|----------------|-----------|--|
| 3   | 1.10033        | -42       | (6, 6, 4, 6, 6, 3, 0, 3, -4)           |
| 4   | 1.11760        | -30       | (0, 0, 0, 3, 3, 2, 3, 0, -1)           |
| 5   | 1.00538        | -56       | (10, 4, 0, 3, 3, 2, 3, 2, 1)           |
| 6   | 1.06750        | -150      | (0, 0, 0, 15, 10, 5, 5, 1, -2)         |
| 7   | 1.02686        | -113      | (8, 6, 0, 5, -4, 4, 3, -3, 3)          |
| 8   | 1.04123        | -120      | (7, 7, 0, 4, -4, 3, 4, -3, 2)          |
| 9   | 1.05142        | -132      | (8, 4, 0, 4, -3, 4, 2, -3, 4)          |
| 10  | 1.06249        | -360      | (25, 8, 7, 10, -9, 8, 8, -7, 6)        |
| 20  | 1.11557        | -840      | (19, 19, 0, 10, -10, 9, 10, -9, 8)     |
| 30  | 1.14292        | -3105     | (70, 23, 22, 25, -24, 23, 23, -22, 21) |
| 40  | 1.15932        | -3480     | (39, 39, 0, 20, -20, 19, 20, -19, 18)  |

*Conclusion.*—We proposed a gradient-based method for optimizing Bell inequalities, demonstrated its effectiveness on PI Bell inequalities involving up to two-body dichotomic correlators, and identified new tight Bell inequalities for the scenario of three measurements per party ( $m = 3$ ). The framework is general and can be extended naturally towards certifying quantumness in

many-body systems [18–20]. It can also be adapted to PI Bell inequalities involving higher-body correlators [31], translationally invariant Bell inequalities [29, 39, 40, 48], and to nonsymmetric Bell inequalities [34, 49–52]. Here we determine the quantum value as the ground-state energy of its corresponding Hamiltonian within the symmetric measurement setting, serving as a variational upper bound, thereby fixing the Hilbert space dimension. A certified lower bound can be established through SDP-based relaxation methods [53, 54], which we leave for future work.

*Acknowledgments.*—We thank Owidusz Makuta and Eloïc Vallée for reading the manuscript and offering helpful comments. J.F.C., M.H., and J.T. acknowledge the support received from the European Union’s Horizon Europe research and innovation programme through the ERC StG FINE-TEA-SQUAD (Grant No. 101040729). This publication is part of the ‘Quantum Inspire - the Dutch Quantum Computer in the Cloud’ project (with project number [NWA.1292.19.194]) of the NWA research program ‘Research on Routes by Consortia (ORC)’, which is funded by the Netherlands Organization for Scientific Research (NWO). Parts of this work were performed by using the compute resources from the Academic Leiden Interdisciplinary Cluster Environment (ALICE) provided by Leiden University. The views and opinions expressed here are solely those of the authors and do not necessarily reflect those of the funding institutions. Neither of the funding institutions can be held responsible for them.

---

\* jinfuchen@lorentz.leidenuniv.nl  
 † mengyao@lorentz.leidenuniv.nl  
 ‡ tura@lorentz.leidenuniv.nl

[1] A. Einstein, B. Podolsky, and N. Rosen, *Physical Review* **47**, 777 (1935).  
 [2] J. S. Bell, *Physics Physique Fizika* **1**, 195 (1964).  
 [3] J. F. Clauser, M. A. Horne, A. Shimony, and R. A. Holt, *Physical Review Letters* **23**, 880 (1969).  
 [4] L. J. Landau, *Foundations of Physics* **18**, 449 (1988).  
 [5] L. Masanes, Necessary and sufficient condition for quantum-generated correlations (2003), arXiv:quant-ph/0309137.  
 [6] B. Hensen, H. Bernien, A. E. Dréau, A. Reiserer, N. Kalb, M. S. Blok, J. Ruitenberg, R. F. L. Vermeulen, R. N. Schouten, C. Abellán, W. Amaya, V. Pruneri, M. W. Mitchell, M. Markham, D. J. Twitchen, D. Elkouss, S. Wehner, T. H. Taminiau, and R. Hanson, *Nature* **526**, 682 (2015).  
 [7] M. Giustina, M. A. M. Versteegh, S. Wengerowsky, J. Handsteiner, A. Hochrainer, K. Phelan, F. Steinlechner, J. Kofler, J.-A. Larsson, C. Abellán, W. Amaya, V. Pruneri, M. W. Mitchell, J. Beyer, T. Gerrits, A. E. Lita, L. K. Shalm, S. W. Nam, T. Scheidl, R. Ursin, B. Wittmann, and A. Zeilinger, *Physical Review Letters* **115**, 250401 (2015).  
 [8] L. K. Shalm, E. Meyer-Scott, B. G. Christensen, P. Bierhorst, M. A. Wayne, M. J. Stevens, T. Gerrits, S. Glancy, D. R. Hamel, M. S. Allman, K. J. Coakley, S. D. Dyer, C. Hodge, A. E. Lita, V. B. Verma, C. Lambrocco, E. Tortorici, A. L. Migdall, Y. Zhang, D. R. Kumor, W. H. Farr, F. Marsili, M. D. Shaw, J. A. Stern, C. Abellán, W. Amaya, V. Pruneri, T. Jennewein, M. W. Mitchell, P. G. Kwiat, J. C. Bienfang, R. P. Mirin, E. Knill, and S. W. Nam, *Physical Review Letters* **115**, 250402 (2015).  
 [9] W. Rosenfeld, D. Burchardt, R. Garthoff, K. Redeker, N. Ortegel, M. Rau, and H. Weinfurter, *Physical Review Letters* **119**, 010402 (2017).  
 [10] S. Storz, J. Schär, A. Kulikov, P. Magnard, P. Kurpiers, J. Lütolf, T. Walter, A. Copetudo, K. Reuer, A. Akin, J.-C. Besse, M. Gabureac, G. J. Norris, A. Rosario, F. Martin, J. Martinez, W. Amaya, M. W. Mitchell, C. Abellán, J.-D. Bancal, N. Sangouard, B. Royer, A. Blais, and A. Wallraff, *Nature* **617**, 265 (2023).  
 [11] A. Acín, N. Brunner, N. Gisin, S. Massar, S. Pironio, and V. Scarani, *Physical Review Letters* **98**, 230501 (2007).  
 [12] S. Pironio, A. Acín, N. Brunner, N. Gisin, S. Massar, and V. Scarani, *New Journal of Physics* **11**, 045021 (2009).  
 [13] U. Vazirani and T. Vidick, *Physical Review Letters* **113**, 140501 (2014).  
 [14] F. Xu, X. Ma, Q. Zhang, H.-K. Lo, and J.-W. Pan, *Reviews of Modern Physics* **92**, 025002 (2020).  
 [15] S. Pironio, A. Acín, S. Massar, A. B. De La Giroday, D. N. Matsukevich, P. Maunz, S. Olmschenk, D. Hayes, L. Luo, T. A. Manning, and C. Monroe, *Nature* **464**, 1021 (2010).  
 [16] A. Fyillas, B. Bourdoncle, A. Mainos, P.-E. Emeriau, K. Start, N. Margaria, M. Morassi, A. Lemaître, I. Sagnes, P. Stepanov, T. H. Au, S. Boissier, N. Somaschi, N. Maring, N. Belabas, and S. Mansfield, *PRX Quantum* **5**, 020348 (2024).  
 [17] C. Zhang, Y. Li, X.-M. Hu, Y. Xiang, C.-F. Li, G.-C. Guo, J. Tura, Q. Gong, Q. He, and B.-H. Liu, *Physical Review Letters* **134**, 090201 (2025).  
 [18] I. Šupić and J. Bowles, *Quantum* **4**, 337 (2020).  
 [19] Y. Li, Y. Xiang, J. Tura, and Q. He, *Physical Review Letters* **135**, 060201 (2025).  
 [20] F. Baccari, R. Augusiak, I. Šupić, J. Tura, and A. Acín, *Physical Review Letters* **124**, 020402 (2020).  
 [21] B. Chazelle, *Discrete & Computational Geometry* **10**, 377 (1993).  
 [22] I. Pitowsky, *Quantum Probability — Quantum Logic*, Lecture Notes in Physics, Vol. 321 (Springer-Verlag, Berlin/Heidelberg, 1989).  
 [23] I. Pitowsky, *Mathematical Programming* **50**, 395 (1991), publisher: Springer.  
 [24] J.-D. Bancal, N. Brunner, N. Gisin, and Y.-C. Liang, *Physical Review Letters* **106**, 020405 (2011).  
 [25] M. Froissart, *Il Nuovo Cimento B* **64**, 241 (1981).  
 [26] I. Pitowsky and K. Svozil, *Physical Review A* **64**, 014102 (2001).  
 [27] J. Tura, R. Augusiak, A. B. Sainz, T. Vértesi, M. Lewenstein, and A. Acín, *Science* **344**, 1256 (2014).  
 [28] J. Tura, A. B. Sainz, T. Vértesi, A. Acín, M. Lewenstein, and R. Augusiak, *Journal of Physics A: Mathematical and Theoretical* **47**, 424024 (2014).  
 [29] Z. Wang, S. Singh, and M. Navascués, *Physical Review Letters* **118**, 230401 (2017).  
 [30] R. Schmied, J.-D. Bancal, B. Allard, M. Fadel,

V. Scarani, P. Treutlein, and N. Sangouard, *Science* **352**, 441 (2016).

[31] J. Guo, J. Tura, Q. He, and M. Fadel, *Physical Review Letters* **131**, 070201 (2023).

[32] C. Marconi, G. Müller-Rigat, J. Romero-Pallejà, J. Tura, and A. Sanpera, *Symmetric quantum states: a review of recent progress* (2025), arXiv:2506.10185 [quant-ph].

[33] J. Wang, S. Paesani, Y. Ding, R. Santagati, P. Skrzypczyk, A. Salavrakos, J. Tura, R. Augusiak, L. Mančinska, D. Bacco, D. Bonneau, J. W. Silverstone, Q. Gong, A. Acín, K. Rottwitt, L. K. Oxenløwe, J. L. O'Brien, A. Laing, and M. G. Thompson, *Science* **360**, 285 (2018).

[34] K. Wang, W. Li, S. Xu, M. Hu, J. Chen, Y. Wu, C. Zhang, F. Jin, X. Zhu, Y. Gao, Z. Tan, Z. Cui, A. Zhang, N. Wang, Y. Zou, T. Li, F. Shen, J. Zhong, Z. Bao, Z. Zhu, Z. Song, J. Deng, H. Dong, X. Zhang, P. Zhang, W. Jiang, Z. Lu, Z.-Z. Sun, H. Li, Q. Guo, Z. Wang, P. Emonts, J. Tura, C. Song, H. Wang, and D.-L. Deng, *Physical Review X* **15**, 021024 (2025).

[35] S. Gómez, D. Uzcátegui, I. Machuca, E. S. Gómez, S. P. Walborn, G. Lima, and D. Goyeneche, *Scientific Reports* **11**, 20489 (2021).

[36] W. Li, M. Hu, K. Wang, S. Xu, Z. Lu, J. Chen, Y. Wu, C. Zhang, F. Jin, X. Zhu, Y. Gao, Z. Cui, A. Zhang, N. Wang, Y. Zou, F. Shen, J. Zhong, Z. Bao, Z. Zhu, P. Zhang, H. Li, Q. Guo, Z. Wang, D.-L. Deng, C. Song, H. Wang, P. Emonts, and J. Tura, *Improved Nonlocality Certification via Bouncing between Bell Operators and Inequalities* (2024), arXiv:2407.12347 [quant-ph].

[37] D.-L. Deng, *Physical Review Letters* **120**, 240402 (2018).

[38] N. Brunner, D. Cavalcanti, S. Pironio, V. Scarani, and S. Wehner, *Reviews of Modern Physics* **86**, 419 (2014).

[39] J. Tura, G. De Las Cuevas, R. Augusiak, M. Lewenstein, A. Acín, and J. Cirac, *Physical Review X* **7**, 021005 (2017).

[40] M. Hu, E. Vallée, T. Seynnaeve, P. Emonts, and J. Tura, *Characterizing Translation-Invariant Bell Inequalities using Tropical Algebra and Graph Polytopes* (2024), arXiv:2407.08783 [quant-ph].

[41] M. Fadel and J. Tura, *Quantum* **2**, 107 (2018).

[42] Z. Wang and M. Navascués, *Proceedings of the Royal Society A: Mathematical, Physical and Engineering Sciences* **474**, 20170822 (2018).

[43] P. Emonts, M. Hu, A. Aloy, and J. Tura, *Physical Review A* **110**, 032201 (2024).

[44] Supplemental Material.

[45] B. Toner and F. Verstraete, *Monogamy of Bell correlations and Tsirelson's bound* (2006), arXiv:quant-ph/0611001.

[46] K. Fukuda, *Cddlib reference manual* (2003).

[47] S. Wagner, R. Schmied, M. Fadel, P. Treutlein, N. Sangouard, and J.-D. Bancal, *Physical Review Letters* **119**, 170403 (2017).

[48] M. Hu and J. Tura, *Tropical contraction of tensor networks as a Bell inequality optimization toolset* (2024), arXiv:2208.02798 [quant-ph].

[49] C. Śliwa, *Physics Letters A* **317**, 165 (2003).

[50] S. López-Rosa, Z.-P. Xu, and A. Cabello, *Physical Review A* **94**, 062121 (2016).

[51] F. Bernards and O. Gühne, *Physical Review A* **104**, 012206 (2021).

[52] F. Bernards and O. Gühne, *Physical Review Letters* **125**, 200401 (2020).

[53] M. Fadel and J. Tura, *Physical Review Letters* **119**, 230402 (2017).

[54] M. Navascués, S. Pironio, and A. Acín, *New Journal of Physics* **10**, 073013 (2008).

# Supplemental Material: Optimizing quantum violation for multipartite facet Bell inequalities

Jin-Fu Chen (陈劲夫)<sup>1, 2, \*</sup> Mengyao Hu (胡梦瑶)<sup>1, 2, †</sup> and Jordi Tura <sup>1, 2, ‡</sup>

<sup>1</sup>*Instituut-Lorentz, Universiteit Leiden, P.O. Box 9506, 2300 RA Leiden, The Netherlands*

<sup>2</sup> *$\langle aQa^L \rangle$  Applied Quantum Algorithms, Universiteit Leiden, The Netherlands*

(Dated: November 12, 2025)

The supplementary material is devoted to providing detailed derivations in the main text. In Section I, we show that the ratio between the quantum value and the classical bound of Bell inequalities attains a local maximum when the inequalities are tight. In Section II, we introduce the basics of permutation-invariant (PI) Bell inequalities for  $(N, m, 2)$  scenario with upto two-body correlators, where each of the  $N$  parties performs one of  $m$  possible measurements with binary outcomes  $\pm 1$ . In Section III, we introduce a gradient-based method that optimizes the coefficients of Bell inequalities to achieve the maximum ratio. We show explicit results for the Clauser-Horne-Shimony-Holt (CHSH) inequalities in Section IV, and for PI Bell Inequalities with  $m = 2$  and  $m = 3$  in Section V.

## I. ILLUSTRATION FOR TIGHT BELL INEQUALITIES AS LOCAL MAXIMA OF THE RATIO

The numerical results (Tables I and II in the main text) show that the tight Bell inequality corresponds to a local maximum of the quantum-to-classical ratio  $\Delta := \beta_Q/\beta_C$ . Here we interpret this observation from the geometric point of view.

In the primal space, we consider a two-dimensional affine projection, as shown in Fig. S1, spanned by tight Bell inequalities. The facet (cyan) appears as an edge of the polygon. When the optimal quantum point (red) is unique, the ratio attains a strict local maximum at the tight Bell inequality, as shown in Fig. S1(a), for example, the CHSH inequality. In contrast, as shown in Fig. S1(b), two neighboring facet Bell inequalities (cyan) attain their maximum at the same quantum point (red dot) for example, the two Bell inequalities  $\alpha_{1,\mu} = (0, 0, 0, 6, 3, 3, 0, 1, -2)$  and  $\alpha_{2,\mu} = (0, 0, 0, 0, 3, 1, 6, 3, -2)$  in the  $(4, 3, 2)$  scenario. Consequently, the ratio remains constant for any convex combination of these two inequalities, and the first derivatives with respect to the coefficients  $\alpha_\mu$  vanish. Figure S1(c) shows trivial facets with the ratio  $\Delta = 1$ , for example, the two Bell inequalities  $\alpha_{1,\mu} = (1, 0, 1, 0, 0)$  and  $\alpha_{2,\mu} = (0, 1, 0, 0, 1)$  in the  $(2, 2, 2)$  scenario.

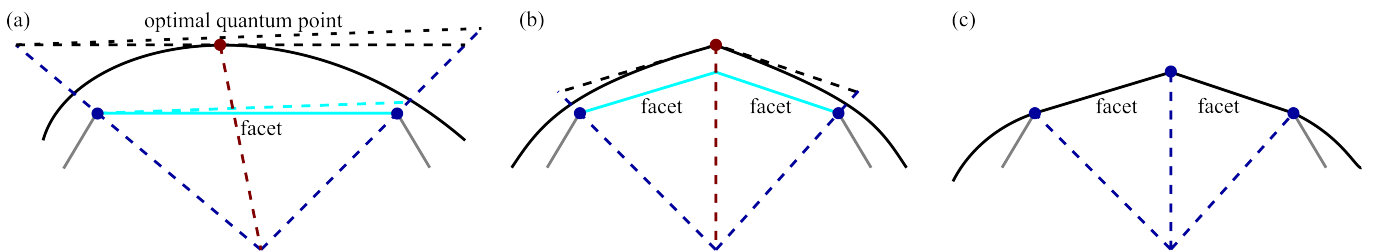


FIG. S1. Illustration of a tight Bell inequality with a local maximum of the ratio. Here we show a two-dimensional affine projection in the primal space of the correlators. (a) For the tight Bell inequality (cyan line), there exists a unique optimal quantum point (red dot), which guarantees that the ratio has a strict local maximum. (b) Two neighboring facet Bell inequalities (cyan lines) share the same optimal quantum point (red dot). Consequently, the ratio is fixed for any convex combination of these two inequalities. (c) Two neighboring facets corresponding to trivial Bell inequalities that do not separate the quantum set from the local polytope.

\* [jinfuchen@lorentz.leidenuniv.nl](mailto:jinfuchen@lorentz.leidenuniv.nl)

† [mengyao@lorentz.leidenuniv.nl](mailto:mengyao@lorentz.leidenuniv.nl)

‡ [tura@lorentz.leidenuniv.nl](mailto:tura@lorentz.leidenuniv.nl)

## II. PERMUTATION-INVARIANT BELL INEQUALITIES FOR $(N, m, 2)$ SCENARIO

To explore the Bell nonlocality in a larger and more complex systems, it is essential to study multipartite Bell inequalities. We consider the  $(N, m, 2)$  Bell scenario, where  $N$  spatially separated parties share an  $N$ -partite resource. Each party can choose one of  $m$  measurements, each yielding two outcomes. We will apply the method of maximizing the ratio between the quantum value and the classical bound for PI Bell inequalities with upto two-body correlators in the  $(N, m, 2)$  scenario.

A PI Bell inequality with upto two body correlators is given by

$$I = \sum_{k=0}^{m-1} \alpha_k \langle \mathcal{S}_k \rangle + \frac{1}{2} \sum_{k,l=0}^{m-1} \alpha_{kl} \langle \mathcal{S}_{kl} \rangle \quad (\text{S1})$$

$$= \sum_{k=0}^{m-1} \alpha_k \langle \mathcal{S}_k \rangle + \frac{1}{2} \sum_{k,l=0}^{m-1} \alpha_{kl} \langle \mathcal{S}_k \mathcal{S}_l - \mathcal{Z}_{kl} \rangle \geq \beta_C, \quad (\text{S2})$$

where the one-body and two-body observables are collected into  $\mathcal{S}_k := \sum_{i=1}^N A_k^{(i)}$  and  $\mathcal{S}_{kl} := \sum_{i \neq j} A_k^{(i)} A_l^{(j)} = \mathcal{S}_k \mathcal{S}_l - \mathcal{Z}_{kl}$  with  $\mathcal{Z}_{kl} := \sum_{i=1}^N (A_k^{(i)} A_l^{(i)} + A_l^{(i)} A_k^{(i)})/2$ . We note that in the equality  $ab = 1 - |a - b| = -1 + |a + b|$  holds for any  $a, b = \pm 1$ . For the classical case we obtain

$$\mathcal{Z}_{kl} = N - \sum_{i=1}^N |A_k^{(i)} - A_l^{(i)}| \quad (\text{S3})$$

$$= -N + \sum_{i=1}^N |A_k^{(i)} + A_l^{(i)}|. \quad (\text{S4})$$

Applying the triangle inequality to Eqs (S3) and (S4), one finds that  $\langle \mathcal{Z}_{kl} \rangle$  is restricted inside a regular tetrahedron [S1]

$$-N + |\langle \mathcal{S}_k \rangle + \langle \mathcal{S}_l \rangle| \leq \langle \mathcal{Z}_{kl} \rangle \leq N - |\langle \mathcal{S}_k \rangle - \langle \mathcal{S}_l \rangle|. \quad (\text{S5})$$

The classical bound  $\beta_C$  is given by the local deterministic strategies corresponding to the vertices of the local polytope  $\mathcal{L}$  in the correlator space. Since the observables have fixed outcomes in the deterministic strategies, the expectation brackets  $\langle \cdot \rangle$  are omitted in the enumeration of vertices. For the vertices,  $\mathcal{S}_k$  and  $\mathcal{Z}_{kl}$  take integer values with the same parity as  $N$ . Since  $I$  depends linearly on  $\mathcal{Z}_{kl}$ , it attains extreme values under the constraint (S5). Therefore, evaluating the classical bound  $\beta_C := \min_{\langle \mathcal{S}_k \rangle, \langle \mathcal{Z}_{kl} \rangle \in \mathcal{L}} I$  requires considering only extreme points on the surfaces of regular tetrahedrons defined by  $(\mathcal{S}_k, \mathcal{S}_l, \mathcal{Z}_{kl})$ .

For the quantum case, we adopt the symmetric measurement setting

$$\hat{A}_k^{(i)} = \cos \theta_k \hat{\sigma}_z^{(i)} + \sin \theta_k \hat{\sigma}_x^{(i)}, \quad (\text{S6})$$

where  $\hat{\sigma}_z^{(i)}$  and  $\hat{\sigma}_x^{(i)}$  are Pauli operators of site  $i$ . The observables  $\hat{\mathcal{S}}_k = \sum_{i=1}^N \hat{A}_k^{(i)}$  can be represented by the collective spin operators

$$\hat{\mathcal{S}}_k = 2 \cos \theta_k \hat{S}_z + 2 \sin \theta_k \hat{S}_x, \quad (\text{S7})$$

where  $\hat{S}_x$ ,  $\hat{S}_y$ , and  $\hat{S}_z$  are the collective spin operators. In the  $\hat{S}_z$  eigenbasis  $|m\rangle : m = N/2, N/2 - 1, \dots, -N/2 + 1, -N/2$ , these matrices are given by

$$(\hat{S}_z)_{m,m'} = m \delta_{m,m'}, \quad (\text{S8})$$

$$(\hat{S}_x)_{m,m'} = \frac{1}{2} \left[ \sqrt{\left(\frac{N}{2} - m'\right) \left(\frac{N}{2} + m' + 1\right)} \delta_{m,m'+1} + \sqrt{\left(\frac{N}{2} + m'\right) \left(\frac{N}{2} - m' + 1\right)} \delta_{m,m'-1} \right], \quad (\text{S9})$$

$$(\hat{S}_y)_{m,m'} = \frac{1}{2i} \left[ \sqrt{\left(\frac{N}{2} - m'\right) \left(\frac{N}{2} + m' + 1\right)} \delta_{m,m'+1} - \sqrt{\left(\frac{N}{2} + m'\right) \left(\frac{N}{2} - m' + 1\right)} \delta_{m,m'-1} \right]. \quad (\text{S10})$$

From Eq. (S7), the operator  $\hat{\mathcal{Z}}_{kl}$  is explicitly given by

$$\hat{\mathcal{Z}}_{kl} = N \cos(\theta_k - \theta_l). \quad (\text{S11})$$

Substituting  $\hat{\mathcal{S}}_k$  and  $\hat{\mathcal{Z}}_{kl}$  into Eq. (S2) gives the Bell operator

$$\hat{I}(\boldsymbol{\theta}) = \sum_{k=0}^{m-1} \alpha_k \hat{\mathcal{S}}_k + \frac{1}{2} \sum_{k,l=0}^{m-1} \alpha_{kl} (\hat{\mathcal{S}}_k \hat{\mathcal{S}}_l - \hat{\mathcal{Z}}_{kl}). \quad (\text{S12})$$

The Bell operator  $\hat{I}(\boldsymbol{\theta})$  depends on the coefficients  $\alpha_{\boldsymbol{\mu}} = \{\alpha_k, \alpha_{kl}\}_{kl}$ , which include both one-body terms  $\alpha_k$  and two-body terms  $\alpha_{kl}$ , and on the measurement settings  $\boldsymbol{\theta} = \{\theta_k\}_k$ . For given coefficients  $\alpha_{\boldsymbol{\mu}}$ , the minimal quantum value  $\beta_Q := \min_{|\psi\rangle, \boldsymbol{\theta}} \langle \psi | \hat{I}(\boldsymbol{\theta}) | \psi \rangle = \min_{\boldsymbol{\theta}} \langle \psi^* | \hat{I}(\boldsymbol{\theta}) | \psi^* \rangle$ , as the ground-state energy of the Hamiltonian  $\hat{I}(\boldsymbol{\theta})$ , is obtained by optimizing the measurement angles  $\boldsymbol{\theta}$ .

### III. GRADIENT-BASED METHOD FOR FINDING TIGHT BELL INEQUALITIES

In this section, we present a gradient-based method for optimizing and tightening Bell inequalities. The key idea is to iteratively adjust coefficients in the inequality to minimize the quantum value while keeping the classical bound fixed, progressively incorporating additional vertices of the local polytope until tightness is achieved.

We consider PI Bell inequalities with up to two-body correlators. Starting from the initial coefficients  $\alpha_{\boldsymbol{\mu}}$ , we consider the set of vertices  $\{\mathcal{S}_{\boldsymbol{\mu},j}\}_j$  that saturate the classical bound  $\beta_C$ , where  $\boldsymbol{\mu}$  labels the correlators and  $j$  indexes the vertices. These vertices  $\mathcal{S}_{\boldsymbol{\mu},j}$  satisfy the constraint

$$\sum_{k=0}^{m-1} \alpha_k \mathcal{S}_{k,j} + \frac{1}{2} \sum_{k,l=0}^{m-1} \alpha_{kl} \mathcal{S}_{kl,j} = \beta_C. \quad (\text{S13})$$

If these saturating vertices  $\{\mathcal{S}_{\boldsymbol{\mu},j}\}_j$  do not span a full-rank affine space, this equation defines a solution space for the coefficients  $\alpha_{\boldsymbol{\mu}}$ . Let  $M = m(m+3)/2$  be the dimension of the correlator space containing the vectors  $\mathcal{S}_{\boldsymbol{\mu}}$ . A Bell inequality is tight if and only if the affine hull of its saturating vertices has dimension  $M-1$ ; Otherwise, the inequality is not tight. For example, for  $(N, 2, 2)$  scenario,  $\mathcal{S}_{\boldsymbol{\mu}} = (\mathcal{S}_0, \mathcal{S}_1, \mathcal{S}_{00}, \mathcal{S}_{01}, \mathcal{S}_{11})$ , and  $M = 5$ .

To explore the solution space of  $\alpha_{\boldsymbol{\mu}}$ , we arrange all the vertices into a matrix  $V$ , which constraint the change of the coefficients as

$$V \delta \alpha_{\boldsymbol{\mu}} = 0. \quad (\text{S14})$$

During the optimization, these constraints [Eq. (S14)] are enforced while maximizing the quantum-to-classical ratio  $\Delta = \beta_Q/\beta_C$ . Within this constrained space, we perform gradient ascent to increase  $\Delta$ , updating the coefficients as

$$\delta \alpha_{\boldsymbol{\mu}} = s [I - V^T (VV^T)^+ V] \frac{\partial \Delta}{\partial \alpha_{\boldsymbol{\mu}}}. \quad (\text{S15})$$

Here  $s$  is the gradient step size;  $\partial \Delta / \partial \alpha_{\boldsymbol{\mu}}$  is the gradient of the ratio;  $I$  is the identity matrix;  $T$  denotes transpose; the superscript  $+$  denotes the Moore-Penrose pseudoinverse [S2, S3]. If the gradient  $\partial \Delta / \partial \alpha_{\boldsymbol{\mu}}$  vanishes in the constraint space, we can replace it with random noise for updating  $\alpha_{\boldsymbol{\mu}}$ .

Our optimization objective is the ratio  $\Delta := \beta_Q/\beta_C$ , whose derivative with respect to  $\alpha_{\boldsymbol{\mu}}$  is generally given by

$$\frac{\partial \Delta}{\partial \alpha_{\boldsymbol{\mu}}} = \frac{1}{\beta_C} \frac{\partial \beta_Q}{\partial \alpha_{\boldsymbol{\mu}}} - \frac{\beta_Q}{\beta_C^2} \frac{\partial \beta_C}{\partial \alpha_{\boldsymbol{\mu}}}. \quad (\text{S16})$$

Both  $\beta_Q$  and  $\beta_C$  vary continuously with  $\alpha_{\boldsymbol{\mu}}$ , but since the constraint in Eq. (S15) keeps  $\beta_C$  fixed, its derivative with respect to  $\alpha_{\boldsymbol{\mu}}$  vanishes within the constraint space. With the Bell operator  $\hat{I}(\boldsymbol{\theta})$  in Eq. (S12), the derivative of the quantum value is obtained as

$$\frac{\partial \beta_Q}{\partial \alpha_{\boldsymbol{\mu}}} = \frac{\partial}{\partial \alpha_{\boldsymbol{\mu}}} \min_{\boldsymbol{\theta}, |\psi\rangle} \langle \psi | \hat{I}(\boldsymbol{\theta}) | \psi \rangle \quad (\text{S17})$$

$$= \frac{\partial}{\partial \alpha_{\boldsymbol{\mu}}} \langle \psi^* | \hat{I}(\boldsymbol{\theta}^*) | \psi^* \rangle \quad (\text{S18})$$

$$= \langle \psi^* | \frac{\partial}{\partial \alpha_{\boldsymbol{\mu}}} \hat{I}(\boldsymbol{\theta}^*) | \psi^* \rangle + \frac{\partial \boldsymbol{\theta}^*}{\partial \alpha_{\boldsymbol{\mu}}} \langle \psi^* | \frac{\partial}{\partial \boldsymbol{\theta}} \hat{I}(\boldsymbol{\theta}) \Big|_{\boldsymbol{\theta}=\boldsymbol{\theta}^*} | \psi^* \rangle \quad (\text{S19})$$

$$= \langle \psi^* | \frac{\partial}{\partial \alpha_{\boldsymbol{\mu}}} \hat{I}(\boldsymbol{\theta}^*) | \psi^* \rangle, \quad (\text{S20})$$

where  $|\psi^*\rangle$  and  $\boldsymbol{\theta}^*$  denote the optimal quantum state and measurement settings. The third equation uses the Feynman–Hellmann theorem since  $|\psi^*\rangle$  is the ground state of the Hamiltonian  $\hat{I}(\boldsymbol{\theta}^*)$ . The fourth equation uses  $\langle\psi^*|\partial_{\boldsymbol{\theta}}\hat{I}(\boldsymbol{\theta})|_{\boldsymbol{\theta}=\boldsymbol{\theta}^*}|\psi^*\rangle=0$ , since  $\boldsymbol{\theta}^*$  minimizes the quantum value.

Once new vertices are identified, they are added to the matrix  $V$ , which may increase the rank of  $V$  and thereby enlarges the subspace spanned by the current vertex set. We then update the coefficients via the projection operator  $I - V^T(VV^T)^+V$  and refine the coefficients  $\alpha_{\boldsymbol{\mu}}$  accordingly. A crucial point is the choice of the gradient step size  $s$ : it must be selected adaptively and kept sufficiently small, so that the trajectory of the coefficients does not cross into other facet of the polytope. By iterating this cycle of projecting, updating, and incorporating new vertices, the procedure gradually refines the inequality until it becomes tight. For clarity, we summarize the constrained gradient update for Bell inequality coefficients in Algorithm 1. In all the numerical cases, the optimization converges to a facet, except for configurations of the type shown in Figs. S1(b) and S1(c). When the gradient vanishes, introducing random noise in the updates of the coefficients  $\alpha_{\boldsymbol{\mu}}$  facilitates eventual convergence to a facet Bell inequality.

---

**Algorithm 1** Constrained Gradient Update for Bell Inequality Coefficients

---

```

1: Input: coefficients  $\alpha_{\boldsymbol{\mu}}^{\text{in}}$ , gradient step size  $s$ , number of parties  $N$ , input vertices  $V^{\text{in}}$ , maximum iteration steps  $K$ 
2: Output: updated coefficients  $\alpha_{\boldsymbol{\mu}}^{\text{out}}$ , output vertices  $V^{\text{out}}$ 
3: if  $\text{rank}(V^{\text{in}}) = d$  then
4:   Return  $(\alpha_{\boldsymbol{\mu}}^{\text{in}}, V^{\text{in}})$ 
5: end if
6:  $V \leftarrow V^{\text{in}}$ 
7:  $\delta\alpha_{\boldsymbol{\mu}}^{\text{try}} \leftarrow s \frac{\partial \Delta}{\partial \alpha_{\boldsymbol{\mu}}} \Big|_{\alpha_{\boldsymbol{\mu}}=\alpha_{\boldsymbol{\mu}}^{\text{in}}}$ 
8: for  $t = 1$  to  $K$  do
9:    $\alpha_{\boldsymbol{\mu}} \leftarrow \alpha_{\boldsymbol{\mu}}^{\text{in}} + [I - V^T(VV^T)^+V]\delta\alpha_{\boldsymbol{\mu}}^{\text{try}}$ 
10:  Evaluate classical bound at  $\alpha_{\boldsymbol{\mu}}$  to get new vertices  $V^{\text{add}}$ 
11:   $V \leftarrow \text{merge}(V, V^{\text{add}})$ 
12:  if  $V^{\text{in}} \subseteq V$  then
13:    Return  $(\alpha_{\boldsymbol{\mu}}, V)$  as  $(\alpha_{\boldsymbol{\mu}}^{\text{out}}, V^{\text{out}})$ 
14:  end if
15: end for
16: Return  $(\alpha_{\boldsymbol{\mu}}, V)$  as  $(\alpha_{\boldsymbol{\mu}}^{\text{out}}, V^{\text{out}})$ 

```

---

#### IV. LOCAL POLYTOPE AND QUANTUM SET FOR (2, 2, 2) SCENARIO

We first consider the (2, 2, 2) scenario as a benchmark to introduce and validate our optimization framework. Our gradient optimization converges to the CHSH inequality in this scenario. The linear functional with only considering the two-body terms is explicitly

$$I = \alpha_{00} \langle A_0 B_0 \rangle + \alpha_{01} \langle A_0 B_1 \rangle + \alpha_{10} \langle A_1 B_0 \rangle + \alpha_{11} \langle A_1 B_1 \rangle, \quad (\text{S21})$$

where  $\langle A_k B_l \rangle$  denotes the two-body correlator between measurement  $A_k$  on Alice and  $B_l$  on Bob satisfying

$$-1 \leq \langle A_k B_l \rangle \leq 1. \quad (\text{S22})$$

The local hidden variable model gives the following constraints on the correlators

$$\begin{aligned} -2 &\leq \langle A_0 B_0 \rangle + \langle A_0 B_1 \rangle + \langle A_1 B_0 \rangle + \langle A_1 B_1 \rangle \leq 2, \\ -2 &\leq \langle A_0 B_0 \rangle - \langle A_0 B_1 \rangle + \langle A_1 B_0 \rangle + \langle A_1 B_1 \rangle \leq 2, \\ -2 &\leq \langle A_0 B_0 \rangle + \langle A_0 B_1 \rangle - \langle A_1 B_0 \rangle + \langle A_1 B_1 \rangle \leq 2, \\ -2 &\leq \langle A_0 B_0 \rangle + \langle A_0 B_1 \rangle + \langle A_1 B_0 \rangle - \langle A_1 B_1 \rangle \leq 2. \end{aligned} \quad (\text{S23})$$

The quantum set of the two-body correlations is represented by [S4, S5]

$$\begin{aligned} -\pi &\leq \arcsin(\langle A_0 B_0 \rangle) + \arcsin(\langle A_0 B_1 \rangle) + \arcsin(\langle A_1 B_0 \rangle) + \arcsin(\langle A_1 B_1 \rangle) \leq \pi, \\ -\pi &\leq \arcsin(\langle A_0 B_0 \rangle) - \arcsin(\langle A_0 B_1 \rangle) + \arcsin(\langle A_1 B_0 \rangle) + \arcsin(\langle A_1 B_1 \rangle) \leq \pi, \\ -\pi &\leq \arcsin(\langle A_0 B_0 \rangle) + \arcsin(\langle A_0 B_1 \rangle) - \arcsin(\langle A_1 B_0 \rangle) + \arcsin(\langle A_1 B_1 \rangle) \leq \pi, \\ -\pi &\leq \arcsin(\langle A_0 B_0 \rangle) + \arcsin(\langle A_0 B_1 \rangle) + \arcsin(\langle A_1 B_0 \rangle) - \arcsin(\langle A_1 B_1 \rangle) \leq \pi. \end{aligned} \quad (\text{S24})$$

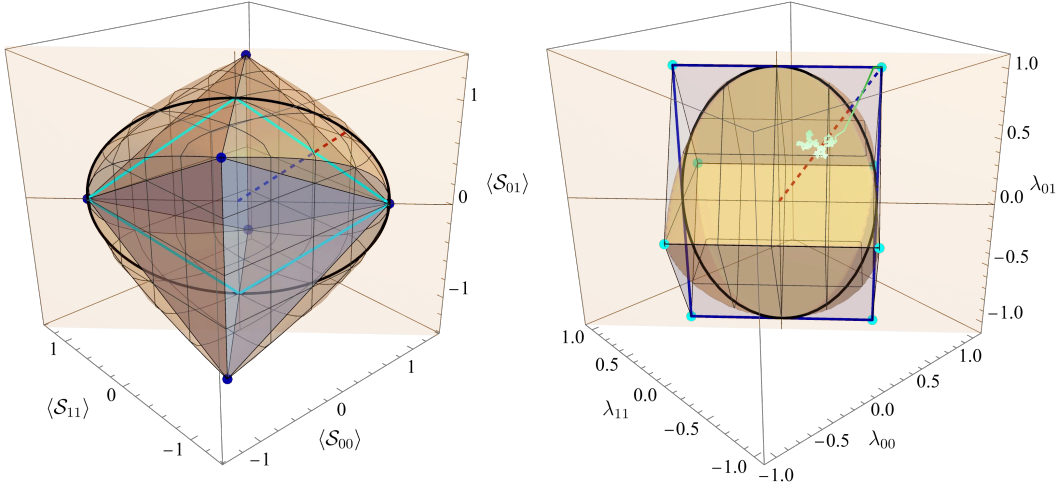


FIG. S2. Local polytope and quantum set for bipartite system. (a) The original local polytope (inside) and quantum set (outside). Four CHSH inequalities correspond to the facets indicated by the blue lines. (b) The dual polytope (outside) and the dual quantum set (inside). The vertices of the polytope are tight Bell inequalities. In both subfigures, the solid curves show a 2D cross section where the largest ratio is obtained. The light-green trajectory shows the convergence of the inequality to one of the CHSH inequalities during the optimization.

Let us consider the symmetric Bell inequality with  $\alpha_{01} = \alpha_{10}$ . We introduce

$$\langle S_{00} \rangle = \langle A_0 B_0 \rangle, \langle S_{01} \rangle = (\langle A_0 B_1 \rangle + \langle A_1 B_0 \rangle)/2, \langle S_{11} \rangle = \langle A_1 B_1 \rangle, \quad (S25)$$

and obtain the symmetric bipartite Bell inequality

$$I = \alpha_{00} \langle S_{00} \rangle + 2\alpha_{01} \langle S_{01} \rangle + \alpha_{11} \langle S_{11} \rangle \geq \beta_C. \quad (S26)$$

Figure S2(a) shows the local polytope (inner octahedron) and the quantum set (outer convex body) for the symmetric  $(2, 2, 2)$  scenario. The local polytope is simplified into

$$|\langle S_{01} \rangle| \leq 1 - |\langle S_{00} \rangle - \langle S_{11} \rangle|/2, \quad (S27)$$

which has six vertices  $(S_{00}, S_{01}, S_{11}) = \pm(1, \pm 1, 1)$  and  $\pm(1, 0, -1)$  (blue dots). The quantum set by Eq. (S24) is simplified into

$$|\langle S_{01} \rangle(\langle S_{00} \rangle - \langle S_{11} \rangle)| \leq (1 - \langle S_{01} \rangle)^{1/2}[(1 - \langle S_{00} \rangle)^{1/2} + (1 - \langle S_{11} \rangle)^{1/2}]. \quad (S28)$$

Four CHSH inequalities with the largest ratio correspond to the facets of the local polytope. In a 2D cross section, the CHSH inequalities are shown by the cyan lines, and the black curves show the quantum value.

Figure S2(b) shows the polar transformation of both the local polytope (outer hexahedron) and the quantum set (inner convex body) by solving the dual variables  $\lambda_{00}$ ,  $\lambda_{01}$ , and  $\lambda_{11}$  from

$$\lambda_{00} \langle S_{00} \rangle + \lambda_{01} \langle S_{01} \rangle + \lambda_{11} \langle S_{11} \rangle \geq -1. \quad (S29)$$

Each tight Bell inequality corresponds to a cyan vertex of the polytope. Four CHSH vertices are  $(\lambda_{00}, \lambda_{01}, \lambda_{11}) = \pm(1/2, -1, \pm 1/2)$ . The other four vertices are  $(\lambda_{00}, \lambda_{01}, \lambda_{11}) = \pm(1, 0, 0)$  and  $\pm(0, 0, 1)$ . The dual quantum set is given by  $\sqrt{(\lambda_{00} - \lambda_{11})^2 + \lambda_{01}^2} \leq 1$  and  $(|\lambda_{00} + \lambda_{11}| + |\lambda_{01}|) \leq 1$ . We also show the two-dimensional cross section that contains the maximum ratio achieved by the CHSH inequalities represented by the four vertices in the cross section. We show the trajectory during optimization in Fig. S2(b) by the green curve; the step size is chosen as  $s = 0.01$ . In the initial stage, when the gradient vanishes ( $\partial \Delta / \partial \alpha_\mu = 0$ ), the gradient term in Eq. (S15) is replaced by random noise sampled from a standard normal distribution. We remark the two-dimensional affine projection and the cross section in both subfigures correspond to Fig. S2 (a) and (b) in the main text.

## V. TIGHT BELL INEQUITIES FOR $(N, 2, 2)$ AND $(N, 3, 2)$ SCENARIOS WITH SMALL $N$

In the following, we focus on finding tight PI Bell inequalities involving up to two-body correlators in the  $(N, m, 2)$  scenario with  $m = 2$  or  $m = 3$ . For  $m = 2$ , the linear functional is explicitly

$$I = \alpha_0 \langle \mathcal{S}_0 \rangle + \alpha_1 \langle \mathcal{S}_1 \rangle + \frac{1}{2} \alpha_{00} (\langle \mathcal{S}_0^2 \rangle - N) + \alpha_{01} (\langle \mathcal{S}_0 \mathcal{S}_1 - \mathcal{Z}_{01} \rangle) + \frac{1}{2} \alpha_{11} (\langle \mathcal{S}_1^2 \rangle - N), \quad (\text{S30})$$

where  $\mathcal{S}_0$ ,  $\mathcal{S}_1$  and  $\mathcal{Z}_{01}$  are classical random variables. To search for tight Bell inequalities, we enumerate the vertices of the local polytope corresponding to local deterministic strategies according to Sec. II. The classical bound  $\beta_C$  is obtained as the minimum value of  $I$  over the vertices.

To evaluate the quantum value, we consider the measurements encoded by Eqs. (S7) and (S11). The Bell operator is given by

$$\hat{I}(\boldsymbol{\theta}) = \alpha_0 \hat{\mathcal{S}}_0 + \alpha_1 \hat{\mathcal{S}}_1 + \frac{1}{2} \alpha_{00} (\hat{\mathcal{S}}_0^2 - N) + \frac{1}{2} \alpha_{01} (\hat{\mathcal{S}}_0 \hat{\mathcal{S}}_1 + \hat{\mathcal{S}}_1 \hat{\mathcal{S}}_0 - 2 \hat{\mathcal{Z}}_{01}) + \frac{1}{2} \alpha_{11} (\hat{\mathcal{S}}_1^2 - N). \quad (\text{S31})$$

Plugging the measurement settings (Eqs. (S7) and (S11)) into Eq. (S31), we obtain

$$\begin{aligned} \hat{I}(\boldsymbol{\theta}) = & 2(\alpha_{00} \cos^2 \theta_0 + 2\alpha_{01} \cos \theta_0 \cos \theta_1 + \alpha_{11} \cos^2 \theta_1) \hat{\mathcal{S}}_x + 2(\alpha_{00} \sin^2 \theta_0 + 2\alpha_{01} \sin \theta_0 \sin \theta_1 + \alpha_{11} \sin^2 \theta_1) \hat{\mathcal{S}}_z^2 \\ & + 2[\alpha_{00} \cos \theta_0 \sin \theta_0 + \alpha_{11} \cos \theta_1 \sin \theta_1 + \alpha_{01} (\sin \theta_0 \cos \theta_1 + \cos \theta_0 \sin \theta_1)] (\hat{\mathcal{S}}_x \hat{\mathcal{S}}_z + \hat{\mathcal{S}}_z \hat{\mathcal{S}}_x) \\ & + 2(\alpha_0 \cos \theta_0 + \alpha_1 \cos \theta_1) \hat{\mathcal{S}}_x + 2(\alpha_0 \sin \theta_0 + \alpha_1 \sin \theta_1) \hat{\mathcal{S}}_z - \frac{1}{2} \alpha_{00} N - \alpha_{01} N \cos(\theta_0 - \theta_1) - \frac{1}{2} \alpha_{11} N. \end{aligned} \quad (\text{S32})$$

The minimal quantum value is obtained by searching over  $\theta_0$  and  $\theta_1$  to minimize the ground state energy of  $\hat{I}(\boldsymbol{\theta})$ .

TABLE I: The ratio and the corresponding coefficients for nontrivial facet Bell inequality for  $N = 4$ ,  $m = 2$ .

| $\Delta_{4,2}$ | $\beta_Q$ | $\beta_C$ | $(\alpha_0, \alpha_1, \alpha_{00}, \alpha_{01}, \alpha_{11})$ |
|----------------|-----------|-----------|---|
| 1.11303        | -20.03447 | -18       | (0, 0, 6, 2, -1)  |
| 1.02579        | -30.77363 | -30       | (12, 3, 6, 2, -1)   |
| 1.01391        | -54.75094 | -54       | (12, 6, 12, 8, -1)  |
| 1.01339        | -42.56235 | -42       | (12, 9, 6, 6, 1)  |

TABLE II: The ratio and the corresponding coefficients for nontrivial facet Bell inequality for  $N = 5$ ,  $m = 2$ .

| $\Delta_{5,2}$ | $\beta_Q$  | $\beta_C$ | $(\alpha_0, \alpha_1, \alpha_{00}, \alpha_{01}, \alpha_{11})$ |
|----------------|------------|-----------|---|
| 1.05904        | -84.72301  | -80       | (20, 4, 20, 5, -2)  |
| 1.01769        | -24.42458  | -24       | (6, 6, 1, 2, 1)   |
| 1.01515        | -10.15146  | -10       | (2, 0, 1, 1, 1)   |
| 1.01117        | -70.78216  | -70       | (20, 14, 5, 5, 1)   |
| 1.00805        | -201.61020 | -200      | (60, 24, 30, 15, -2)  |
| 1.00747        | -130.97171 | -130      | (36, 28, 8, 10, 3)  |
| 1.00679        | -161.08648 | -160      | (60, 12, 20, 5, -2)   |
| 1.00138        | -400.55077 | -400      | (60, 36, 60, 45, 2)   |

TABLE III: The ratio and the corresponding coefficients for nontrivial facet inequalities for  $N = 6$ ,  $m = 2$

| $\Delta_{6,2}$ | $\beta_Q$ | $\beta_C$ | $(\alpha_0, \alpha_1, \alpha_{00}, \alpha_{01}, \alpha_{11})$ |
|----------------|-----------|-----------|---|
| 1.05884        | -63.53040 | -60       | (0, 0, 15, 3, -1)   |
| 1.02444        | -92.19967 | -90       | (30, 5, 15, 3, -1)  |
| 1.02153        | -12.25837 | -12       | (2, 0, 1, 1, 1)   |
| 1.01628        | -16.26044 | -16       | (4, 2, 1, 1, 1)   |

(continued on next page)

| (continued from previous page) |            |           |   |
|--------------------------------|------------|-----------|---|
| $\Delta_{6,2}$                 | $\beta_Q$  | $\beta_C$ | $(\alpha_0, \alpha_1, \alpha_{00}, \alpha_{01}, \alpha_{11})$ |
| 1.01616                        | -42.67892  | -42       | (9, 9, 1, 2, 1)   |
| 1.00870                        | -121.04430 | -120      | (30, 20, 5, 5, 1)   |
| 1.00804                        | -226.80917 | -225      | (54, 41, 8, 10, 3)  |
| 1.00740                        | -157.15448 | -156      | (37, 17, 23, 12, 1)   |
| 1.00616                        | -112.69001 | -112      | (26, 12, 17, 9, 1)  |
| 1.00544                        | -48.26112  | -48       | (13, 5, 4, 3, 2)  |
| 1.00517                        | -165.85362 | -165      | (40, 20, 20, 12, 1)   |
| 1.00471                        | -24.11309  | -24       | (5, 1, 3, 2, 1)   |
| 1.00408                        | -39.15927  | -39       | (12, 3, 4, 2, 1)  |
| 1.00381                        | -195.74390 | -195      | (60, 20, 20, 8, -1)   |
| 1.00290                        | -240.69671 | -240      | (45, 15, 45, 18, -1)  |
| 1.00224                        | -70.15691  | -70       | (18, 12, 3, 3, 1)   |
| 1.00216                        | -180.38922 | -180      | (60, 10, 15, 3, -1)   |
| 1.00138                        | -300.41277 | -300      | (0, 0, 45, 27, 1)   |
| 1.00065                        | -129.08436 | -129      | (24, 20, 12, 12, 5)   |
| 1.00041                        | -273.11285 | -273      | (60, 32, 36, 24, 5)   |

For  $m = 2$ , the `cddlib` [S6] is used to enumerate facets of the local polytope, and the ratio  $\Delta_{N,2}$  is evaluated for each facet Bell inequality. Our gradient optimization converges to one facet Bell inequality. For  $N = 3$ , there is a single nontrivial facet Bell inequalities  $(6, 2, 6, 3, -2)$  with the maximum ratio  $\Delta_{3,2}^{\max} = 1.11303$ . We present in Tables I, II, and III the ratios for all nontrivial facet Bell inequalities in the  $(N, 2, 2)$  scenario for  $N = 4, 5$ , and 6, respectively. We find 4, 8, and 20 inequalities with the ratio  $\Delta_{N,2} > 1$ . For  $N = 5$  and 6, the ratio of the facet Bell inequality  $(2, 0, 1, 1, 1)$  is larger than 1. As the number of parties  $N$  increases, this Bell inequality continues to achieve the maximum ratio when compared against all facet Bell inequalities within the fixed  $(N, 2, 2)$  scenario.

For the  $(N, 3, 2)$  scenario, the linear functional is

$$I = \alpha_0 \langle \mathcal{S}_0 \rangle + \alpha_1 \langle \mathcal{S}_1 \rangle + \alpha_2 \langle \mathcal{S}_2 \rangle + \frac{1}{2} \alpha_{00} (\langle \mathcal{S}_0^2 \rangle - N) + \frac{1}{2} \alpha_{11} (\langle \mathcal{S}_1^2 \rangle - N) + \frac{1}{2} \alpha_{22} (\langle \mathcal{S}_2^2 \rangle - N) + \alpha_{01} (\langle \mathcal{S}_0 \mathcal{S}_1 - \mathcal{Z}_{01} \rangle) + \alpha_{02} (\langle \mathcal{S}_0 \mathcal{S}_2 - \mathcal{Z}_{02} \rangle) + \alpha_{12} (\langle \mathcal{S}_1 \mathcal{S}_2 - \mathcal{Z}_{12} \rangle), \quad (\text{S33})$$

and the Bell operator  $\hat{I}(\theta)$  is constructed similarly to Eq. (S31) by introducing  $\hat{\mathcal{S}}_0 = 2 \cos \theta_0 \hat{S}_z + 2 \sin \theta_0 \hat{S}_x$ ,  $\hat{\mathcal{S}}_1 = 2 \cos \theta_1 \hat{S}_z + 2 \sin \theta_1 \hat{S}_x$ ,  $\hat{\mathcal{S}}_2 = 2 \cos \theta_2 \hat{S}_z + 2 \sin \theta_2 \hat{S}_x$ ,  $\hat{\mathcal{Z}}_{01} = N \cos(\theta_0 - \theta_1)$ ,  $\hat{\mathcal{Z}}_{02} = N \cos(\theta_0 - \theta_2)$ , and  $\hat{\mathcal{Z}}_{12} = N \cos(\theta_1 - \theta_2)$ .

We list the ratios over all the facet Bell inequalities with  $N \leq 4$  using `cddlib` [S6]. The results of the ratio and the nontrivial facet Bell inequalities are given in Tables. IV, V, and VI for  $N = 2, 3$ , and 4, respectively. For  $N = 2$  and 3, the maximum ratio for  $m = 3$  is the same as that for  $m = 2$ , but a larger ratio is obtained when  $N \geq 4$ . For  $N = 4$ , the ten largest ratios and their corresponding coefficients are shown. The Bell inequality with  $\alpha_{\mu} = (0, 0, 0, 3, 3, 2, 3, 0, -1)$  has a larger ratio  $\Delta_{4,3}^{\max} = 1.11760$  compared to  $\Delta_{4,2}^{\max} = 1.11303$  by  $\alpha_{\mu} = (0, 0, 6, 2, -1)$ . Since `cddlib` [S6] becomes infeasible for larger values of  $N$ , we instead employ our gradient-based method to search for Bell inequalities and obtain the inequalities listed in Table II of the main text.

TABLE IV: The ratio and the corresponding coefficients for nontrivial facet Bell inequalities for  $N = 2, m = 3$ .

| $\Delta_{2,3}$ | $\beta_Q$    | $\beta_C$ | $(\alpha_0, \alpha_1, \alpha_2, \alpha_{00}, \alpha_{01}, \alpha_{02}, \alpha_{11}, \alpha_{12}, \alpha_{22})$ |
|----------------|--------------|-----------|--|
| $\sqrt{2}$     | $-2\sqrt{2}$ | -2        | (0, 0, 0, 1, 1, 0, -1, 0, 0)   |
| $\sqrt{2}$     | $-4\sqrt{2}$ | -4        | (0, 0, 0, 0, 1, 1, 0, 1, -2)   |
| $5/4$          | -10          | -8        | (2, 1, 1, 2, 2, 2, -2, 1, -2)  |

TABLE V: The ratio and the corresponding coefficients for nontrivial facet Bell inequalities for  $N = 3, m = 3$ .

| $\Delta_{3,3}$ | $\beta_Q$ | $\beta_C$ | $(\alpha_0, \alpha_1, \alpha_2, \alpha_{00}, \alpha_{01}, \alpha_{02}, \alpha_{11}, \alpha_{12}, \alpha_{22})$ |
|----------------|-----------|-----------|--|
| 1.11303        | -20.03447 | -18       | (4, 2, 2, 2, 2, 0, 1, -2)  |

(continued on next page)

(continued from previous page)

| $\Delta_{3,3}$ | $\beta_Q$ | $\beta_C$ | $(\alpha_0, \alpha_1, \alpha_2, \alpha_{00}, \alpha_{01}, \alpha_{02}, \alpha_{11}, \alpha_{12}, \alpha_{22})$ |
|----------------|-----------|-----------|--|
| 1.11303        | -20.03447 | -18       | (6, 2, 0, 6, 3, 0, -2, 0, 0)   |
| 1.10033        | -46.21398 | -42       | (6, 6, 4, 6, 6, 3, 0, 3, -4)   |
| 1.09643        | -52.62880 | -48       | (12, 6, 2, 12, 6, 0, 0, 3, -2)   |
| 1.09545        | -32.86344 | -30       | (6, 6, 2, 3, 3, 3, 0, -2)  |
| 1.09395        | -32.81848 | -30       | (6, 4, 2, 4, 4, 3, 2, 0, -2)   |
| 1.07606        | -22.59729 | -21       | (6, 2, 0, 6, 2, 1, 0, -1, -1)  |
| 1.07157        | -16.07351 | -15       | (2, 2, 0, 2, 2, 1, 2, -1, -1)  |
| 1.06941        | -38.49887 | -36       | (6, 4, 2, 6, 6, 3, -2, 2, -2)  |
| 1.05448        | -15.81716 | -15       | (4, 2, 0, 3, 1, 1, 1, -1, -1)  |
| 1.05099        | -63.05926 | -60       | (6, 6, 4, 12, 9, 6, -2, 4, -4)   |
| 1.04734        | -21.99416 | -21       | (6, 2, 0, 6, 1, 2, 0, -1, -1)  |
| 1.03970        | -11.43666 | -11       | (2, 2, 0, 2, 0, 1, 2, -1, -1)  |
| 1.03825        | -37.37713 | -36       | (4, 2, 2, 8, 5, 5, -2, 2, -2)  |
| 1.03806        | -37.37011 | -36       | (12, 4, 4, 6, 3, 3, -2, 1, -2)   |
| 1.02985        | -30.89545 | -30       | (6, 2, 0, 3, 3, 3, -2, 3, 3)   |
| 1.02831        | -30.84942 | -30       | (6, 2, 0, 4, 3, 4, -2, 2, 2)   |
| 1.02498        | -30.74945 | -30       | (4, 2, 2, 0, 4, 2, 6, 3, -2)   |
| 1.01935        | -36.69651 | -36       | (10, 4, 0, 9, 1, 4, 1, -2, -2)   |
| 1.00897        | -36.32307 | -36       | (6, 2, 0, 2, 3, 4, -2, 4, 6)   |

TABLE VI: The ten largest ratio and the corresponding coefficients for nontrivial facet Bell inequalities for  $N = 4$ ,  $m = 3$ .

| $\Delta_{4,3}$ | $\beta_Q$  | $\beta_C$ | $(\alpha_0, \alpha_1, \alpha_2, \alpha_{00}, \alpha_{01}, \alpha_{02}, \alpha_{11}, \alpha_{12}, \alpha_{22})$ |
|----------------|------------|-----------|--|
| 1.11760        | -33.52793  | -30       | (0, 0, 0, 3, 3, 2, 3, 0, -1)   |
| 1.11303        | -20.03447  | -18       | (0, 0, 0, 6, 2, 0, -1, 0, 0)   |
| 1.11303        | -40.06894  | -36       | (0, 0, 0, 6, 3, 3, 0, 1, -2)   |
| 1.11303        | -20.03447  | -18       | (0, 0, 0, 1, 2, 1, 1, 1, -1)   |
| 1.09879        | -72.52003  | -66       | (0, 0, 0, 18, 6, 0, 0, 2, -1)  |
| 1.09672        | -92.12404  | -84       | (0, 0, 0, 12, 9, 5, 0, 3, -4)  |
| 1.09661        | -65.79685  | -60       | (0, 0, 0, 6, 6, 4, 1, 3, -3)   |
| 1.09594        | -414.26432 | -378      | (9, 6, 3, 42, 39, 24, 6, 17, -19)  |
| 1.09457        | -637.03913 | -582      | (12, 12, 6, 60, 60, 36, 12, 28, -29)   |
| 1.09373        | -413.43150 | -378      | (12, 6, 0, 12, 20, 36, -19, 24, 36)  |

---

[S1] J. Tura, R. Augusiak, A. B. Sainz, T. Vértesi, M. Lewenstein, and A. Acín, *Science* **344**, 1256 (2014).  
 [S2] E. H. Moore, *Bull. Amer. Math. Soc.* **26**, 394 (1920).  
 [S3] R. Penrose, *Mathematical Proceedings of the Cambridge Philosophical Society* **51**, 406 (1955).  
 [S4] L. J. Landau, *Foundations of Physics* **18**, 449 (1988).  
 [S5] L. Masanes, “Necessary and sufficient condition for quantum-generated correlations,” (2003), arXiv:quant-ph/0309137.  
 [S6] K. Fukuda, “Cddlib reference manual,” (2003).